13

# Metamaterial Transmission Line and its Applications

Changjun Liu and Kama Huang
*School of Electronics and Information Engineering,*
Sichuan University, *China*

## 1. Introduction

Metamaterial structures have found a wide interest around the world since the properties of left-handed media were proposed for the first time in 1967 by a Soviet physicist Veselago. Besides many successful investigations on three-dimensional metamaterials, e.g. invisible cloaks and perfect lens, there are many researches on two-dimensional and one-dimensional metamaterials. Homogeneous negative index transmission lines or left-handed transmission lines are, generally speaking, metamaterial transmission lines, which belong to one-dimensional metamaterials. They do not exist in nature, and have to be approached by some artificial structures, which are usually constructed from a series of discontinuous sections operating in a restricted frequency range.

A typical realization of metamaterial transmission line is found in a quasi-lumped transmission line with elementary cells consisting of a series capacitor and a shunt inductor. As in practice, the normal shunt capacitance and series inductance cannot be avoided, the concept of the composite right/left-handed (CRLH) transmission line was developed, and a number of novel applications have been demonstrated.

In this chapter, we focus on metamaterial transmission line designs and applications. Firstly, the concept of metamaterial transmission line is introduced briefly. Secondly, the circuit models, which facilitate the analysis of metamaterial transmission lines, are discussed. The relations between composite right/left-handed transmission line and band-pass filters are analyzed. Finally, some applications of metamaterial transmission lines in microwave components, e.g. diplexers, baluns, and power dividers, are presented.

## 2. Basic models

### 2.1 Full circuit models

The equivalent circuit model of a conventional right-handed transmission line is shown in Fig. 1(a). It consists of series inductors and shunt capacitors, of which the dimensions are much less than the wavelength of the operating frequency. It is well known that many important characteristics, such as characteristic impedance, phase velocity, dispersions and so on, can be obtained from the circuit model.

The equivalent circuit model of a left-handed transmission line is shown in Fig. 1(b), which is a dual of Fig. 1(a). All series inductors in the right-handed transmission line model are replaced by capacitors in the left-handed transmission line model, and all shunt capacitors are substituted by inductors. It is an ideal model, which does not exist in nature.


(a) Pure right-handed transmission line (b) Pure left-handed transmission line

Fig. 1. Equivalent circuit model of right-handed and left-handed transmission line

A composite right/left-handed transmission line model, as shown in Fig. 2, is more suitable than the left-handed transmission line circuit model, since the parasite series inductance and shunt capacitance cannot be avoided in nature. It consists of series resonators $L_R$ and $C_L$ and shunt resonators $C_R$ and $L_L$, where the subscript "L" and "R" denote left-handed and right-handed, respectively. This transmission line circuit model is a combination of left-handed and right-handed transmission line. At low frequency, $C_L$ and $L_L$ are dominant, the transmission line shows left-handed characteristics; at high frequency, $L_R$ and $C_R$ are dominant, the transmission line shows right-handed characteristics.

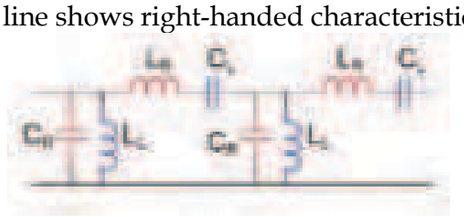

Fig. 2. Equivalent circuit model of composite right/left-handed transmission line

There is no band-gap between left-handed and right-handed regions, if a so-called balanced condition is satisfied. The balanced condition is

$$L_L C_R = L_R C_L \tag{1}$$

which implies the series and shunt LC resonators have the same resonant frequency – transition frequency - $\omega_0$. The characteristic impedance of the composite right/left-handed transmission line is

$$Z_E = Z_L = Z_R \tag{2}$$

where $Z_L = \sqrt{\frac{L_L}{C_L}}$ and $Z_R = \sqrt{\frac{L_R}{C_R}}$ are the pure left-handed and right-handed characteristic impedances which are frequency independent with the homogenous transmission line approach. The cut-off frequencies of the composite right/left-handed transmission line is

$$\begin{cases} \omega_{cL} = \omega_R \left( \sqrt{1 + \frac{\omega_L}{\omega_R}} - 1 \right) \\ \omega_{cR} = \omega_R \left( \sqrt{1 + \frac{\omega_L}{\omega_R}} + 1 \right) \end{cases} \tag{3}$$

where $\omega_L = \frac{1}{\sqrt{L_L C_L}}$ and $\omega_R = \frac{1}{\sqrt{L_R C_R}}$ are the resonant frequencies of the left-handed and right-handed LC circuit, respectively. The transition frequency can be written as

$$\omega_0^2 = \omega_{cL}\omega_{cR} = \omega_L\omega_R = \frac{1}{\sqrt{L_L L_R C_L C_R}} \tag{4}$$

Considering the degree of freedom in the composite right/left-handed transmission line design with periodic elements, there are four parameters, namely $L_L$, $C_L$, $L_R$, and $C_R$. When the balanced condition is applied, there are only three independent parameters left. Once two cut-off frequencies and the characteristic impedance $Z_E$ (matching to the system impedance $Z_0$) are fixed, a unique CRLH TL configuration is determined

$$\begin{cases} \omega_0 L_R = \dfrac{1}{\omega_0 C_L} = \dfrac{\omega_0}{\omega_{cR} - \omega_{cL}} 2Z_0 \\ \omega_0 C_R = \dfrac{1}{\omega_0 L_L} = \dfrac{\omega_0}{\omega_{cR} - \omega_{cL}} \dfrac{2}{Z_0} \end{cases} \tag{5}$$

### 2.2 Relation between filters and metamaterial transmission line models

The circuit model of a composite right/left-handed transmission line is very close to a high order band-pass filter, as shown in Fig. 3. The circuit model is a periodic structure, while a band-pass filter is usually not. However, for high order Chebyshev filters, the central part is a periodic structure as well. Are there some relations between circuit models of Chebyshev filters and composite right/left-handed transmission line? We review the standard band-pass filter design procedure and reveal the relation between them.

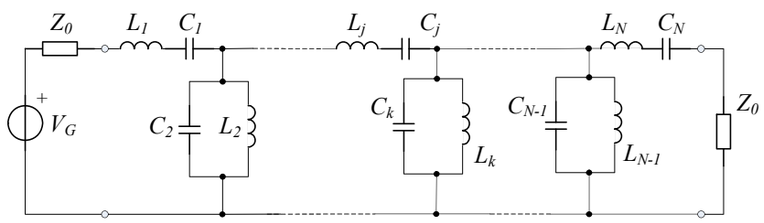


Fig. 3. Equivalent circuit of a band-pass filter

An $N^{th}$ order band-pass filter in principle has the same LC circuit model. The band-pass filter design is usually achieved from the low-pass to band-pass transformation, in which a low-pass prototype filter is applied. The mapping formulas is

$$\begin{cases} \omega_0 L_j = \dfrac{1}{\omega_0 C_j} = \dfrac{\omega_0}{\omega_2 - \omega_1} g_j Z_0 & \text{for series resonators} \\ \omega_0 C_k = \dfrac{1}{\omega_0 L_k} = \dfrac{\omega_0}{\omega_2 - \omega_1} \dfrac{g_k}{Z_0} & \text{for shunt resonators} \end{cases} \tag{6}$$

where $g_i$ is the $i^{th}$ element value (either the inductance or the capacitance) in a prototype low-pass filter, $\omega_1$ and $\omega_2$ are the lower and higher cut-off frequencies, respectively, and $\omega_0 = \sqrt{\omega_1\omega_2}$ is the central frequency of the band-pass filter. $Z_0$ is the system impedance.

Once these parameters are fixed, the band-pass filter is uniquely determined. From Eq. (6), it can be obtained

$$L_j C_j = L_k C_k = \frac{1}{\omega_0^2} \tag{7}$$

which means that the balanced condition of a composite right/left-handed transmission line always holds in a band-pass filter design. Since the mapping formula is a generic formula, it may be applied to other kinds of prototype LPF as well. Thus the balanced case of a composite right/left-handed transmission line is automatically realized in band-pass filters from any kind of prototype low-pass filter with series and shunt LC resonators that are built from the mapping formula Eq. (6). Butterworth, Gaussian, or Chebyshev band-pass filters with any pass-band ripple constructed from Eq. (6) will satisfy the balanced condition of a composite right/left-handed transmission line. In most prototype low-pass filters, the element values $g_i$ usually vary in a certain range and lead to a non-periodic structure. The central section of a high order Chebyshev filter, however, has a periodic structure and is very close to a CRLH TL. Fig. 4 shows an example of a 21st order Chebyshev prototype LPF with different pass-band ripples. For elements not close to either end, the element values are periodic. It should be noted that always two adjacent filter elements form one equivalent transmission line cell, thus the central part of a Chebyshev is a periodic structure, independently of the ripple.

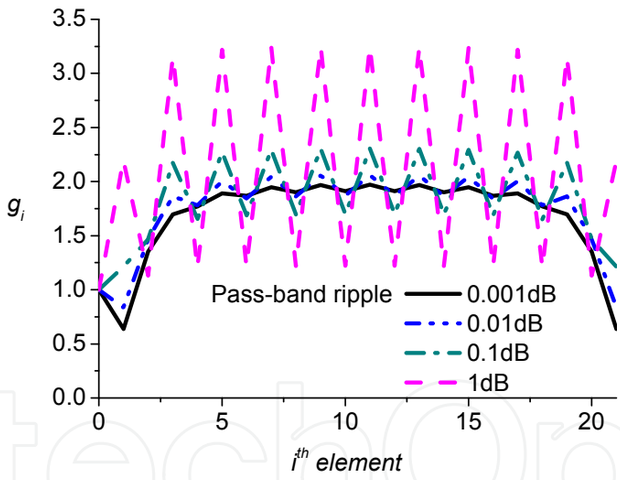


Fig. 4. Element values of 21st order Chebyshev prototype low-pass filters

As shown in Fig. 4, the lower the pass-band ripple, the smoother are the element values. In the limiting case, the values of the central elements are close to $g_i$=2. Moreover, the higher the filter order, the better is the approach to a periodic structure. When the element value is 2, Eq. (5) and Eq. (6) are same. Thus, when the Chebyshev band-pass filter and the composite right/left-handed transmission line have the same cut-off frequencies ($\omega_1 = \omega_{cL}$, $\omega_2 = \omega_{cH}$) and system impedance $Z_0$, they will own the same LC circuit determined by Eq. (5) and Eq. (6), respectively. This implies that once three parameters (two cut-off frequencies and the matching impedance) are fixed, the corresponding composite right/left-handed

transmission line in the balanced case and the central part of the corresponding high order Chebyshev BPF with low pass-band ripple have identical LC configurations.
Once two cut-off frequencies and the system impedance are given, a uniform composite right/left-handed transmission line in the balanced case and a high order Chebyshev band-pass filter with low pass-band ripple can be uniquely implemented with LC circuit, respectively. The composite right/left-handed transmission line and the central part of the Chebyshev BPF own the same periodic LC structures. In other words, a uniform composite right/left-handed transmission line in the balanced case can be considered a part of a high-order low-ripple Chebyshev band-pass filter with the same cut-off frequencies and system impedance.
Therefore, it has been proved that a composite right/left-handed transmission line - in the balanced case - is identical to the central part of a high-order low pass-band ripple Chebyshev band-pass filter with the same characteristic impedance and cut-off frequencies. Theoretically the composite right/left-handed transmission line can be analyzed as a special band-pass filter.
There is an extra parameter in Chebyshev band-pass filters – the pass-band ripples. The central part of a high-ripple high-order Chebyshev band-pass filter is equivalent to a composite right/left-handed transmission line with mismatched impedance to the source and load. With similar analysis, a dual-composite right/left handed transmission line can be regarded as a part of a high order Chebyshev band-stop filter with low pass-band ripples. Thus, the relations between composite right/left handed transmission lines and filters have been presented. The negative phase velocity exists in filters for a long time. But it has not been studied as in a metamaterial transmission line. The discussion on the relations between filters and composite right/left-handed transmission lines give one more freedom in metamaterial transmission line design. It helps the impedance matching, e.g. achieving a broader pass-band with better frequency responses near cut-off frequencies. It helps the design of metamaterial transmission lines from classical filter theory.

## 3. Implementations of metamaterial transmission lines

### 3.1 Composite right/left-handed transmission line realization

A common metamaterial transmission line is a composite right/left-handed transmission line, which is shown in Fig. 5. It is a periodic structure, which consists of series capacitors, i.e. interdigital capacitors, and shunt inductors, i.e. short-ended microstrip lines. There are series inductors and shunt capacitors as well due to the parasite effects. The dimension of each unit should be much less than the guided wavelength, e.g. $p < \lambda_g/5$ . Otherwise, it cannot approach a transmission line from discrete units.

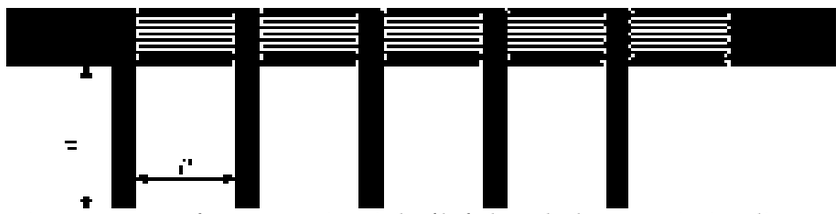

Fig. 5. Microstrip structure of a composite right/left-handed transmission line

The balanced condition can be achieved by adjusting the series and shunt resonators, respectively. The bandwidth of this structure is much limited. The pass-band of upper frequency branch becomes worse due to the self-resonance of the interdigital capacitors. The frequency response of the right-handed region is not as good as the left-handed region. The other drawback is the high insertion loss of the metamaterial transmission line from the interdigital capacitors and the radiation from shunt short-ended microstrip lines.
A microstrip directional coupler at 2.45 GHz is shown in Fig. 6 . It is composed of a composite right/left-handed transmission line (the lower one) and a conventional microstrip transmission line (the upper one). Tight coupling is achieved in this coupler. It is a quasi-zero dB directional coupler, which means all incident power is coupled instead of being transmitted. The structure of the composite right/left-handed transmission line is as in Fig. 5.

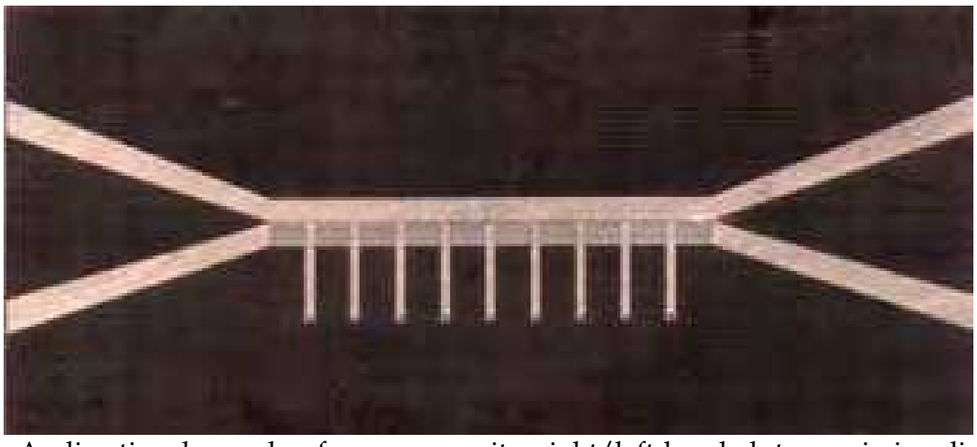

Fig. 6. A directional coupler from composite right/left-handed transmission line and conventional microstrip transmission line

At the transition frequency, there is a phenomenon called zeroth order resonance. The metamaterial transmission line share the same phase and the phase velocity goes to zero, which implies the wavelength is infinite. However, the group velocity is not zero and the incident power can be delivered.
The composite right/left-handed transmission line has found many successful applications, and extends the performance of conventional microwave components.

### 3.2 Composite right/left-handed transmission lines with lumped elements

Based on the theory of composite right/left-handed transmission line and the LC circuit network, a composite right/left-handed transmission line using surface mounted capacitors and short-ended microstrip lines is available. The interdigital capacitors are replaced by lumped capacitors, e.g. ATC chip capacitors. With chip capacitors, a higher series capacitance is easier to reach, and the metamaterial transmission line is more compact. Moreover, the limitation of self-resonance of interdigital capacitors has been released, and a better frequency response can be achieved. A composite right/left-handed transmission line with lumped capacitors is shown in Fig. 7. Six chip capacitors and five short-ended microstrip lines comprise a section of metamaterial transmission line.

The substrate of the metamaterial transmission line is F4B-2 with relative dielectric constant 2.65 and thickness 1 mm. Six chip capacitors are ATC600S series with 0603 package. The capacitance of the capacitor at each end is 5.6 pF, and the capacitance of the capacitors in between is 1.8 pF. The dimension of the microstrip line is: $l_{RH}$ = 5.14 mm, $w_{RH}$ = 2.78 mm, $l_{ind}$ = 9.47 mm, and $w_{ind}$ = 1 mm.

Fig. 7. A composite right/left-handed transmission line with lumped capacitors and the microstrip structure

The performance of the composite right/left-handed transmission line is fabricated and measured with Agilent N5230A vector network analyzer. The amplitude and phase response are shown in Fig. 8. Its bandwidth is from 1 GHz to 5 GHz while the center frequency is at 2.97 GHz, at which there is no phase shifting. When the frequency is between 1 GHz and 2.97 GHz, it works in the left-handed mode ($\beta < 0$); when the frequency is between 2.97 GHz and 5 GHz, it works in the right-handed mode ($\beta > 0$).

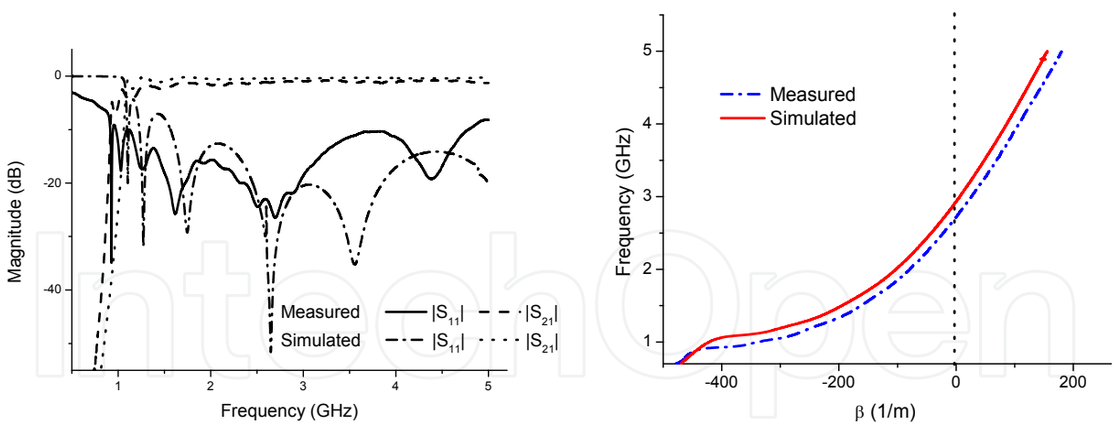


Fig. 8. Amplitude and dispersion of the metamaterial transmission line

This composite right/left-handed transmission line is compact and easy to fabricate, and the insertion loss is less than 1.3 dB, and the return loss is greater than 10 dB. Measurements agree well with simulation results. A broad pass-band is achieved with this metamaterial transmission line. The shortcoming of this metamaterial transmission line is that the performance is strongly dependent on the chip capacitors, which makes the cost higher as well.

## 4. Applications of metamaterial transmission lines

Metamaterial transmission lines have been applied to many fields successfully. They may extend the performance of conventional microwave components due their unique dispersion characteristics. On the other aspect, they may reduce the dimensions of some conventional microwave components greatly. In the fowling, several applications of metamaterial transmission line are presented.

### 4.1 Leaky-wave antenna

The kernel of the leaky-wave antenna is a metamaterial transmission line, which is built by microstrip multilayer structure. It contains two RT/Duroid 5880 substrates with relative dielectric constant $\varepsilon_r$=2.2 of thickness 0.254 mm and 1.58 mm, respectively. Microstrip resonators are uniformly and alternatively distributed in the top and the middle layer, as shown in Fig. 9, to form the equivalent series capacitance and shunt inductance required by the metamaterial transmission line. All microstrip resonators are identical. The unite element is a symmetric microstrip patch with length 16.8mm and width 7.4mm. Those unit elements in dash line, e.g. with number 2 and 4, are located in the middle layer, and those in solid line, e.g. with number 1, 3, and 5, are in the top layer. Therefore, a periodic microstrip structure is applied to approaching the uniform metamaterial transmission line.

The series capacitance in the metamaterial transmission line is from the overlapping between two unit elements in the top and the middle layer respectively. The overlapping region between them is 2.2mm, and the distance between them is 3.8mm. The distance between two adjacent elements is much less than the guided wavelength at the operating frequency. When the feeding is in balanced mode, the metamaterial transmission lines work in the odd mode as two parallel transmission lines. The symmetric plane of the metamaterial transmission line becomes a virtual ground due to the symmetry of the whole structure. The series inductance is from the unavoidable parasite effects and the width variation of the microstrip as well. The shunt inductance and capacitance are provided by the vertical branch connected to the virtual ground.

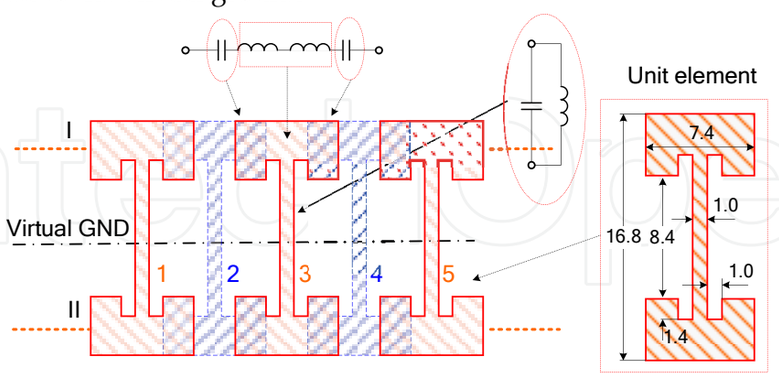


Fig. 9. Structure of the metamaterial transmission line with the equivalent circuits and the dimension of one unit element (© 2007 IEEE)

One segment of the above metamaterial transmission line is applied to build a resonator to analyze its characteristics. Two 1 mm gap capacitors are applied to feed the segment of the metamaterial transmission line at both ends, and make it resonate under the under-coupling

situations. The metamaterial transmission line resonator has been simulated by the Sonnet software to obtain resonant frequencies. The simulated results of $|S_{21}|$ are shown in Fig. 10, where the number of unit elements in the metamaterial transmission line is from one to nine with only odd numbers.

The resonant frequency of one isolated unit element was 3.42 GHz, which increased to 3.95 GHz when more unit elements were coupled together. The zeorth order resonant frequency was between 3.3 GHz to 4.1 GHz. With the increase of the number of unit elements, the zeroth order resonant frequency approached to around 4 GHz, and fixed there. When there were more unit elements coupled together in the metamaterial transmission line, it was possible to obtain the resonance of the metamaterial transmission line in the left-handed or right-handed mode with dominant or high order modes. In the left-handed resonance region, the resonant frequency increased with the increase of the number of unit elements, since the guided wavelength increases with the increase of frequency in left-handed region.

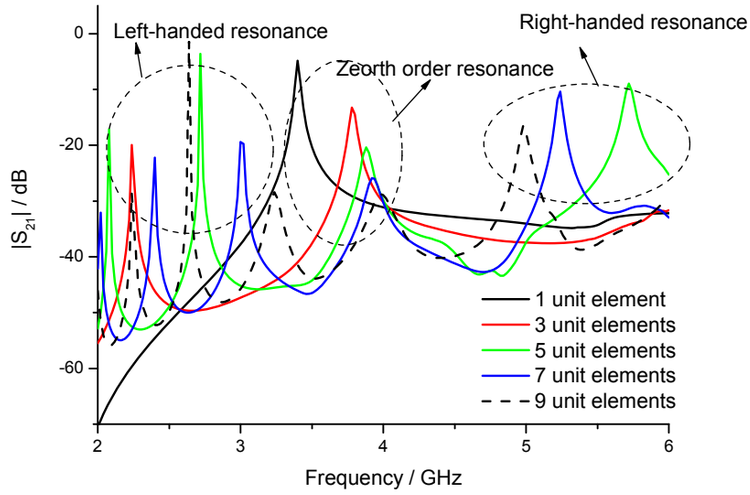


Fig. 10. Simulated resonant frequencies of the NRI TL of different unit elements

At the matched situation, in which the source and load are matched to the characteristic impedance of the metamaterial transmission line with appropriate coupling. All unit elements share the same phase at the zeroth order resonant frequency since the wavelength is infinite. The metamaterial transmission line with 21 unit elements was simulated. At $f_0 = 4.08\,\text{GHz}$ the phase difference between any unit elements was zero, as shown in Fig. 11. It was also worth noticing that: a) the phase difference between any two unit elements became greater when frequency was farther away from $f_0$; b) the phase difference relation reversed (from advanced to delayed or versus) when frequency changed from $f < f_0$ to $f_0 < f$ .

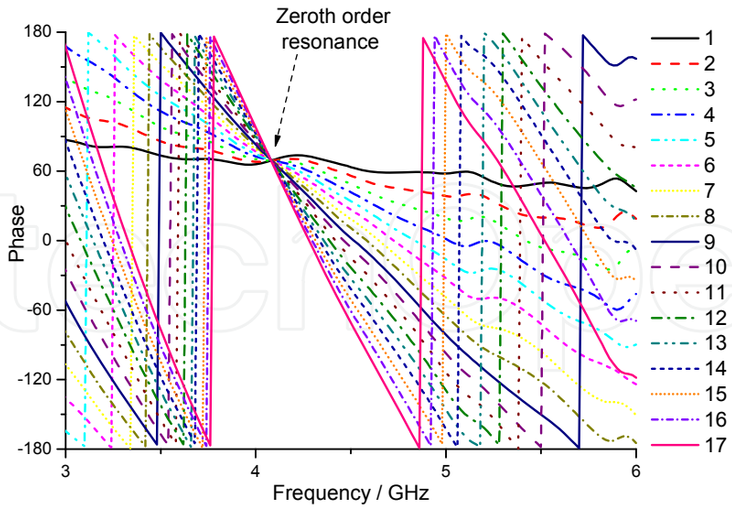


Fig. 11. Phase distribution among the NRI TL with 17 unit elements which are numerated from 1 to 17 (© 2007 IEEE)

The dispersion of the metamaterial transmission line with 17 unit elements is obtained from the simulated phase difference between the source and the load. The results are as shown in Fig. 12. In the left-handed dominant region $f < f_0$, the wavelength increases with the increase of frequency. At the centre frequency $f = f_0$, the wavelength is infinite. In the right-handed dominant region $f > f_0$, the wavelength degreases with the increase of frequency.

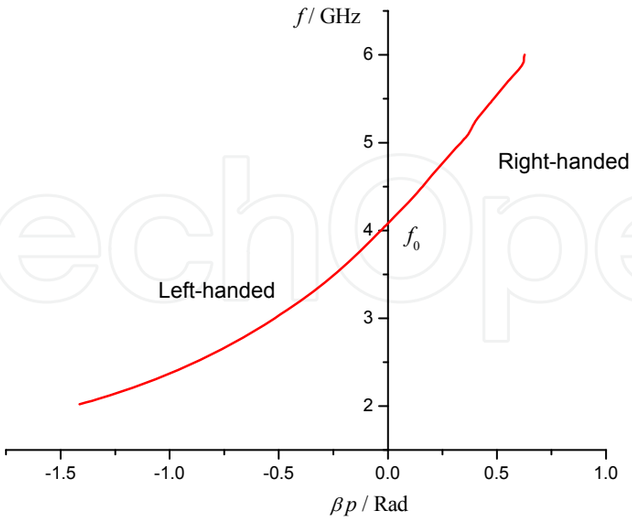


Fig. 12. Simulated dispersion of the metamaterial transmission line with 17 unit elements where p is the length of one unit element. The transition frequency between dominant left-handed and right-handed is 4.08 GHz.

The metamaterial transmission line should be fed in a balanced mode with reversed phases. Therefore, a balun is required to feed the metamaterial transmission line by coaxial lines. Since the metamaterial transmission line has a good performance and may tolerance the amplitude and phase variation, the requirement on the balun performance is low. To build a compact balun, we integrated the balun directly to the metamaterial transmission line. The balun is directly integrated into the negative index transmission lines with two attached microstrip stubs which lead to a very compact antenna feeding system.

The frequency scanned leaky-wave antenna contains the balun, the metamaterial transmission line, and the matched load, as shown in Fig. 13. When the metamaterial transmission line is fed by reversed phase microwave signals with equal amplitudes, a virtual ground occurs in the symmetry plane. The advantage of this constellation is that it does not require any vias to build the shunt inductors. Moreover, it has a broader bandwidth and potential applications in higher frequency band compared to the implementation with interdigital capacitors, since the resonance from those interdigital capacitors has been removed.


(a) Top metallization layer

(b) Middle metallization layer

Fig. 13. Leaky-wave metamaterial antenna with 21 and 22 unit elements on the top and in the middle metallization layer, respectively. The bottom layer is the ground. The feeding port is a 50 Ω microstrip line connected to a SMA connector (© 2007 IEEE).

As shown in Fig. 14, the reflections introduced by each unit element have zero phase shifts at the center frequency and add up coherently at the feeding port, leading to an increased $|S_{11}|$ at the central frequency. On the other hand, the ripple of the reflection is obvious. It is caused by the periodic nature of the leaky-wave antenna based on metamaterial transmission lines.

The novel leaky-wave antenna is designed on the metamaterial transmission line. The antenna comprises 30 elements, and the total size with the integrated microstrip balun is about 200 mm by 20 mm. Each element contains a pair of inductors and capacitors. The antenna works at C-band from about 3.5 GHz to 5.5 GHz with a return loss smaller than 10 dB. In the operating frequency range, the main beam scanning angle is from -45° to 45°. The antenna gain is higher than 10 dB in this frequency range. All side lobe levels are more than 10 dB below the main beam at all scanning angles. Simulated antenna patterns are shown in Fig. 15.

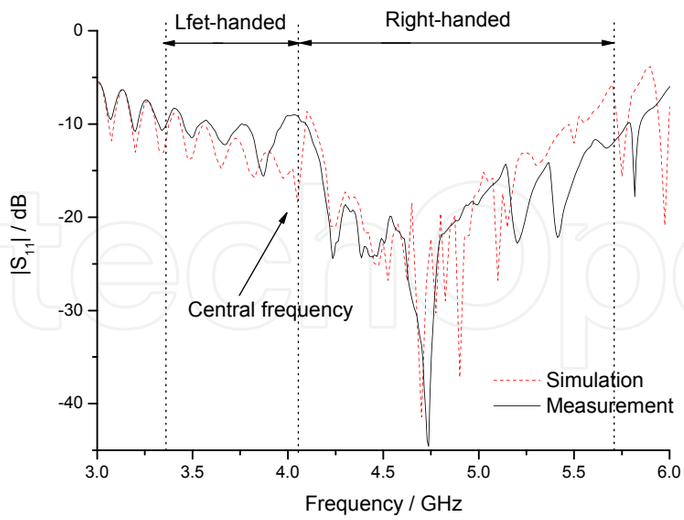


Fig. 14. Measured and simulated voltage reflection coefficients of the leaky-wave antenna. The operating band is from about 3.3 GHz to 5.7 GHz. The central frequency is 4.15 GHz, at which the reflection is slightly higher.

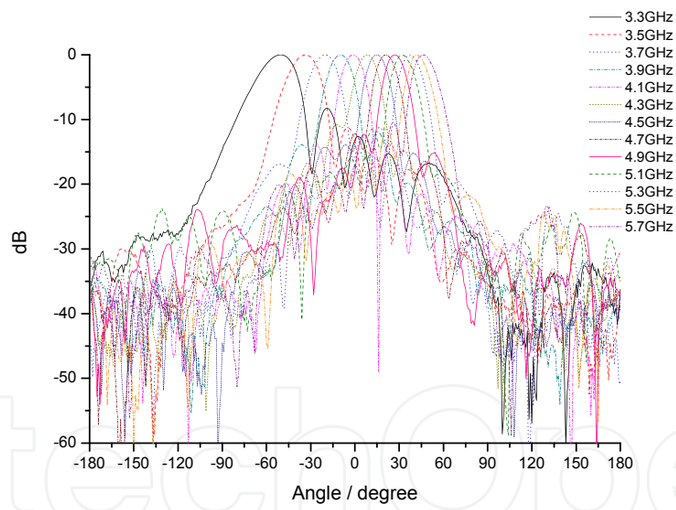


Fig. 15. Measured antenna radiation patterns on the H-plane from 3.3 GHz to 5.7 GHz, in which the main beam scans from about -40° to 40°. All side lobes are lower than -10 dB. The beam-widths at low frequencies are wider than those at high frequencies (© 2007 IEEE).

The leaky-wave frequency scanned antenna based on metamaterial transmission lines is composed of two metamaterial transmission lines with a two-layer structure, a balun and a load. It steers main beam from end-fire to back-fire from -40° to 40° with the antenna gain about 10 dB. It is a compact structure due to the integrated balun. It exhibits a good performance at C band from 3.3 GHz to 5.7 GHz. Meanwhile, it can be extended to high frequency band application since it owns no vias.

### 4.2 Balun

The principle structure of the proposed balun is shown in Fig. 16, in which the dimensions of one unit are presented. Each unit contains a series interdigital capacitor and a narrow shunt microstrip branch. At the dashed line in Fig. 16, the balun may be divided into two identical symmetric parts, namely the upper part and the lower part. In the example of Fig. 16, there are five units in either part.

When port I and II are fed with opposite phase and identical amplitude, and port III and IV are connected to matched loads, the odd mode will be excited in the symmetric structure. An electric wall is formed in the symmetry plane along the dashed line, forming a virtual ground. A similar metamaterial transmission line structure has been reported in antenna applications. Then, the vertical microstrip branches of length $a$ are equivalent to shunt inductors. The upper part and the lower part become a pair of coupled metamaterial transmission lines. The pass-band of the balun is determined by the metamaterial transmission lines, which is between the cut-off frequencies of the left-handed and right-handed modes. The characteristic impedance of the metamaterial transmission line is equal to $Z_C$.

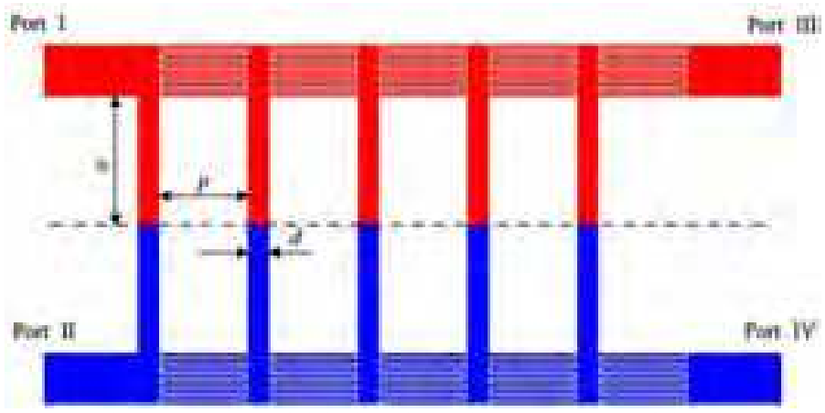


Fig. 16. Structure of the metamaterial balun based on metmaterial transmission lines. The gap between fingers of an interdigital capacitor is 0.10 mm, and the width of fingers is 0.15 mm. Other dimensions are: $a$ = 6.05 mm, p = 4.2 mm, and d = 1 mm (© 2008 IEEE).

When port I and II are fed with identical amplitude and phase, the even mode will be excited in the balun. A magnetic wall, equivalent to open circuits, is formed in the symmetry plane. In this case, however, the vertical microstrip branches turn from short-ended to open-ended. The previous pass-band for the odd mode becomes a stop-band.

Odd and even mode equivalent circuits and their combination are shown in Fig. 17 (a), (b), and (c), respectively. In the combined case, port I is the unique input port. Port III and IV are output ports. The odd mode is supported in the pass-band of the metamaterial transmission line, while the even mode sees a stop-band and is suppressed. There is only the odd-mode left in the output resulting in identical amplitude and opposite phase at ports III and IV. Thus, the proposed design works well as a balun, with the unbalanced input at port I and the balanced outputs between ports III and IV.

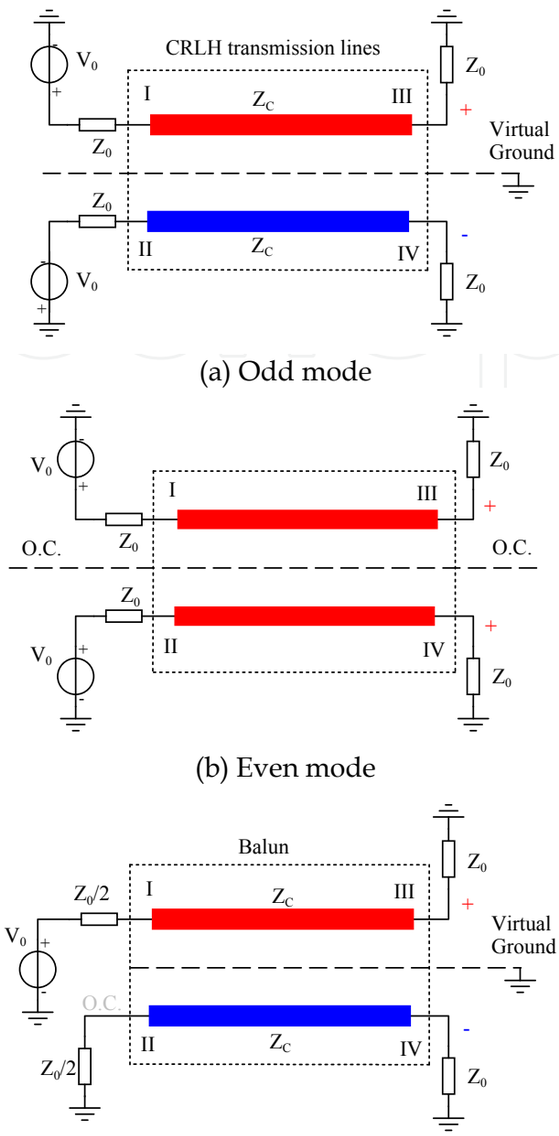


(a) Odd mode

(b) Even mode

(c) Combination of the odd and even mode

Fig. 17. Odd and even mode equivalent circuits and their combination (© 2008 IEEE)

In the proposed balun, the source impedance is required to be half of the load impedance. In applications and measurements, input/output impedances are usually $Z_0$. Therefore, the characteristic impedance $Z_C$ of the metamaterial transmission line should be either $2Z_0$ or $Z_0$, and impedance matching circuits have to be involved in either output or input port. A trade-off is to choose the impedance $Z_C$ between $2Z_0$ and $Z_0$, and apply short transition microstrip lines for impedance matching at both input and output ports.

When port III and IV are matched, port I and II are isolated against each other. When port I is the input port, port II may be an open circuit. The matching load at port II can be omitted. To keep the structure symmetric, a section of open-ended microstrip line is kept at port II. In the case of mismatched loads are applied at the output ports, a matched load at port II

should be used. Moreover, based on the relation between Chebyshev band-pass filters and metamaterial transmission lines, the first and last units of the metamaterial lines are adjusted to achieve better impedance match and wider bandwidth.
Following the above steps, we have designed and optimized two baluns from metamaterial transmission lines with five and seven units, shown in Fig. 18 (a) and (b), namely balun A and B, respectively. The substrate material is RT Duroid 5880 of thickness of 1.57 mm and a relative dielectric constant of $\varepsilon_r = 2.2$. All input and output ports are matched to $Z_0 = 50\ \Omega$.

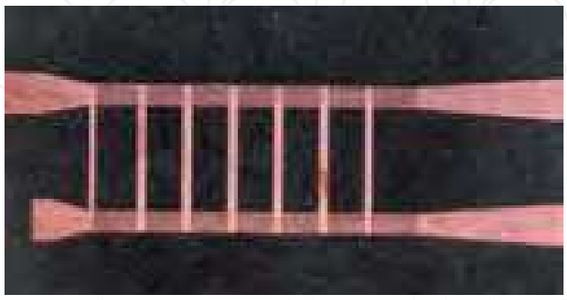

Fig. 18. Photos of a baluns based on metamaterial transmission lines. The balun is of sizes of about 65 mm × 35 mm (© 2008 IEEE).

The baluns were measured using a HP 8510C vector network analyzer. Simulated and measured results have good agreements for both amplitudes and phases, as shown in Fig. 19.
The output amplitude difference is less than 0.7 dB, and either insertion loss is smaller than 5 dB from 1.6 GHz to 4.0 GHz. The return loss is greater than 10 dB. The phase difference between the two output ports is between 178° and 184° (181° ±3°) within the frequency range from 1.5 GHz to 3.6 GHz.

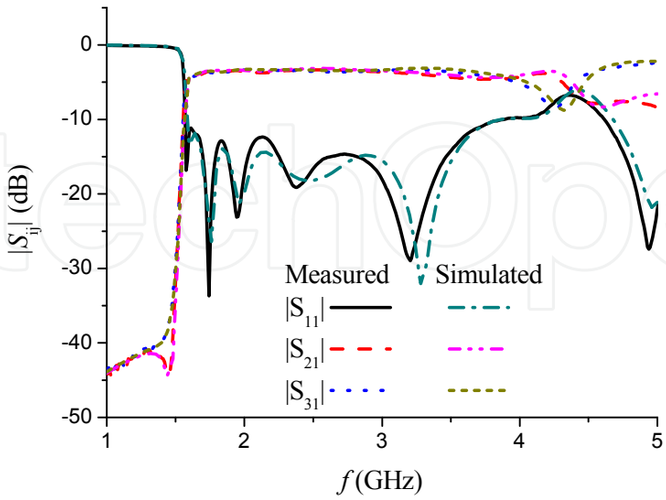


(a) Return loss and transmission performance of balun B

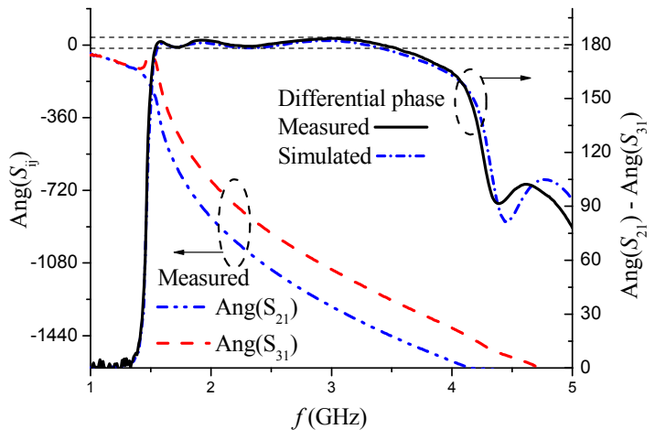


(b) Measured differential phase of balun B

Fig. 19. Simulated and measured results of baluns A and B

The novel broadband metamaterial balun design has been demonstrated. No vias and power dividers are used. Two baluns with five and seven units, respectively, have been fabricated, measured, and compared. Simulations show a good agreement with measured results. The bandwidth of the balun is from about 1.6 GHz to 3.6 GHz, while the output balance is better than 0.7 dB, and the differential phase is 181° ±3°.

### 4.3 Diplexer

A microstrip realization of dual-composite right/left-handed transmission line is shown in Fig. 20. The parallel LC resonator is composed of a interdigital capacitor ($C_L$) and a short narrow microstrip line ($L_R$). The series LC resonator is composed of a small patch ($C_R$) and a short narrow microstrip line ($L_L$). LC components are adjusted at both ends to achieve better impedance match and bandwidth.

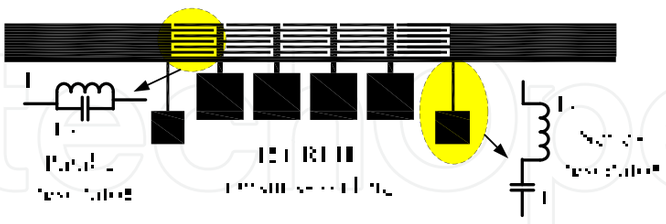

Fig. 20. Configuration of a dual-composite right/left-handed (D-CRLH) transmission line

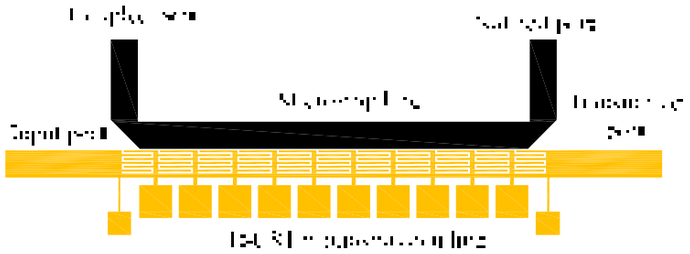

(b) Configuration of the coupler

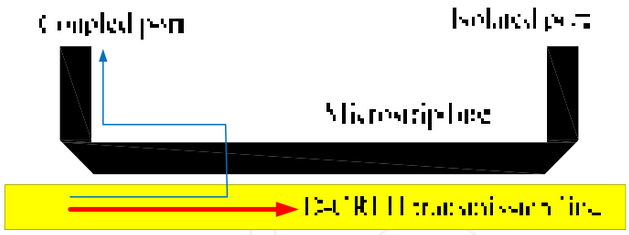

(c) Coupler in the right-handed mode

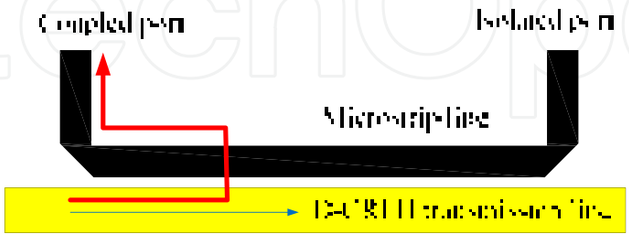

(d) Coupler in the left-handed mode

Fig. 21. Directional coupler from dual-composite right/left-handed transmission lines (© 2009 IEEE)

A conventional microstrip line and a dual-composite right/left-handed transmission line parallel to each other to form a directional coupler, as shown in Fig. 21 (a). The demonstrated D-CRLH transmission line contains twelve unit elements.

It is a dual-band directional coupler, which works at both right-handed and left-handed regions. However, the coupling coefficients are much different from each other. When the frequency is below the band-gap, it works in the right-handed mode and a weak coupling is obtained, as shown in Fig. 21 (b). On the other hand, when the frequency is above the band-gap, it works in the left-handed region and a strong coupling is achieved, as shown in Fig. 21 (c).

The coupling coefficient difference between the left-handed and right-handed modes can be higher than 20 dB in the above design. If the coupling coefficient is nearly 0 dB at the left-handed mode, it may reach 20 dB at the right-handed mode. Thus, microwave at different frequencies are transmitted to different ports dependent on its modes.

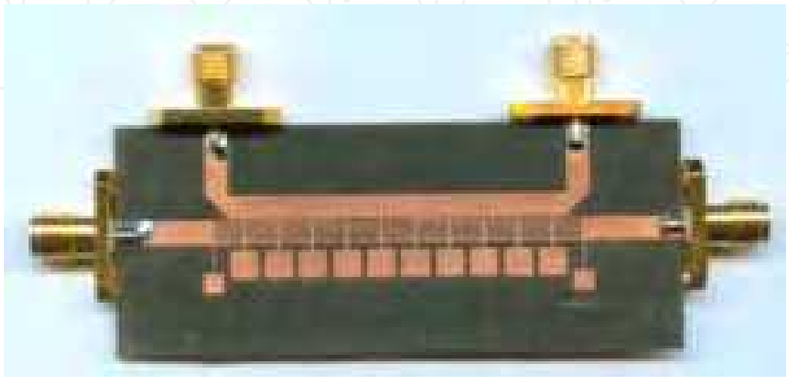

Fig. 22. Fabricated diplexer (© 2009 IEEE)

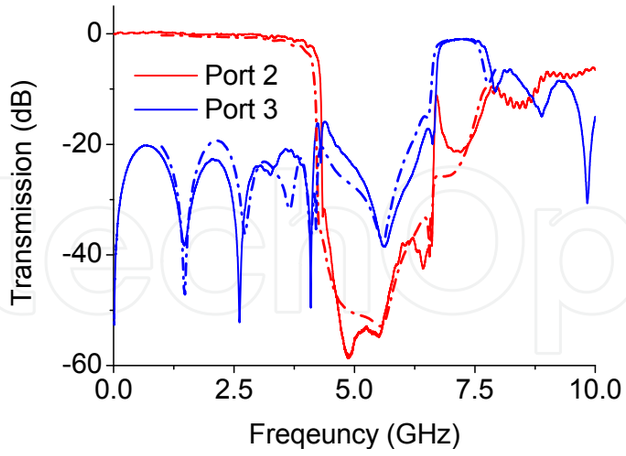


(a) Transmission

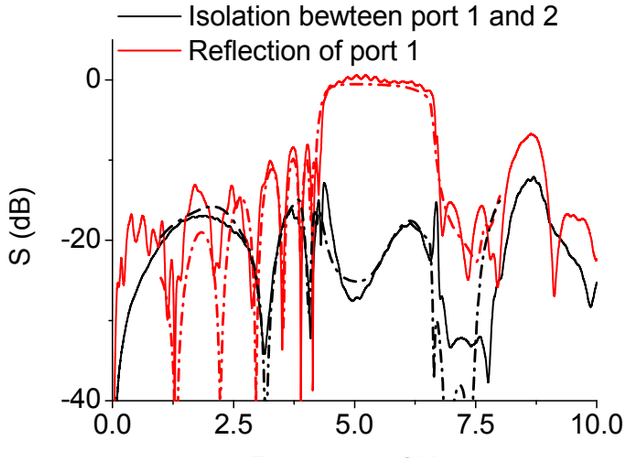


(b) Isolation and reflection

Fig. 23. Simulated and measured results. Simulated and measured results are in solid lines and dashed lines, respectively (© 2009 IEEE).

The fabricated diplexer is shown in Fig. 22, which contains a D-CRLH transmission line and a conventional microstrip line. There are twelve unit elements in the D-CRLH transmission line to achieve 0 dB coupling in the left-handed mode. The diplexer is fabricated on FB4-2 substrate with dielectric constant of 2.65 and thickness of 1 mm. The thickness of copper foils of both sides is 0.017 mm. The dimension of the diplexer is about 65 mm by 25 mm. All spacings and finger widths of interdigital capacitors are 0.2 mm, and the length of each interdigital capacitor is 3.27 mm. The inductor LR is formed by short microstrip lines with width 0.4 mm. The capacitor CR is a rectangle patch with dimension 3.4 mm by 3.4 mm. The inductor LL is formed by microstrip line with width of 0.4 mm and length of 0.8 mm. The distance between the conventional and the D-CRLH transmission lines is 0.15 mm.

Port 1 to port 4 are the input port, the transmitted port, the coupled port, and the isolated port, respectively. Measurements have been performed by Agilent E8362B vector microwave network analyzer. The measured results are shown in Fig. 23 with solid lines. Simulations have been performed by Zeland IE3D, and are shown in Fig. 23 with dashed lines. Simulated results agree well with measured results.
The transmission characteristic of the diplexer is shown in Fig. 23(a). When the frequency is below 3.7 GHz, microwave is delivered to port 2 with an insertion loss less than 1 dB. Due to the parasitic effects of interdigital capacitors, there is a upper frequency limitation for the D-CRLH transmission line. In the proposed design, it is about 7.6 GHz. Thus, when the frequency is from 6.8 GHz to 7.6 GHz, microwave is transferred to port 3 with an insertion loss less than 1.7 dB.
The rejection band of the diplexer is from about 4.4 GHz to 6.6 GHz as shown in Fig. 23(b). The isolation between port 2 and port 3 is higher than 20 dB in lower frequency band, and greater than 35 dB in higher frequency band. A quite high isolation is achieved over a wide frequency band, e.g. from DC up to 3.7 GHz.

### 4.4 Power divider

Fig. 24 shows a symmetrical microstrip dual-composite right/left-handed transmission line structure. This structure is a planar configuration constituted of four unit cells. Each cell includes an interdigital capacitor and several simple microstrip elements. The fundamental four LC parameters ($L_R$, $L_L$, $C_R$, $C_L$) of the metamaterial transmission line are obtained by the conditions of $Z_0 = 50\Omega$, $f_{cR} = 4.5$ GHz and $f_{cL}=6.5$ GHz. The capacitance $C_R$ and the inductance $L_R$ and $L_L$ are implemented as simple microstrip elements, the capacitance $C_L$ is implemented as interdigital capacitor.

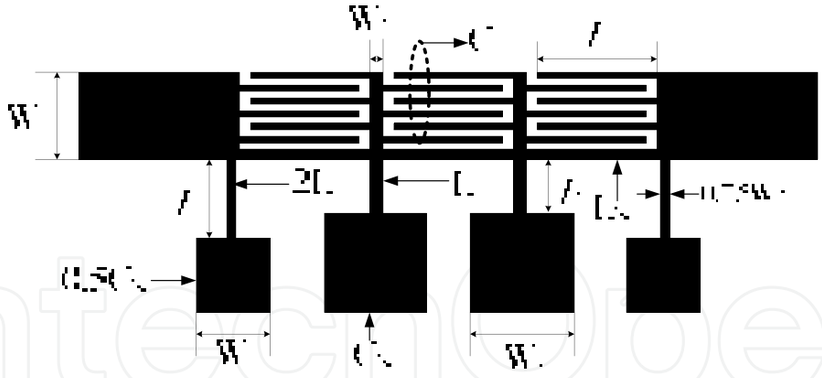

Fig. 24. Layout of the dual-composite right/left-handed transmission line

The substrate is F4B-2 with $\varepsilon_r$=2.65 and h =1 mm. The system impedance is Z0 = 50 Ω, and $W_1$ = 2.8 mm. The characteristic impedance of $L_R$ and $L_L$ are 125 Ω, which is a reasonable value to realize a microstrip inductor. $W_2$ = 0.4 mm is obtained. The width of $2L_L$ is set to 0.75 $W_2$, and the characteristic impedance is 136 Ω.
The proposed 3dB D-CRLH transmission line power divider is the one shown in Fig. 25, where each branch of the divider is a balanced D-CRLH line. In theory, the power divider contains the same two wide pass-band as the D-CRLH transmission line: the low frequency right-handed pass-band (from DC to cut-off frequency $f_{cR}$), and the high frequency left-handed pass-band (from cut-off frequency $f_{cL}$ to unlimitedly high-frequency). But in

practice, the bandwidth of the matching network cannot be made wide enough to cover the whole left-handed and right-handed pass-band, and the performance of the D-CRLH transmission line is poor at high frequency band due to radiation loss and parasitic effects. However, the performance of the D-CRLH transmission line is perfect at the low frequency right-handed pass-band. Thus, we use the right-handed pass-band of the D-CRLH transmission line for power divider design, in which a wideband fourth order Chebyshev matching transformers is applied as well. The microstrip line length of each order is $\lambda_g/4$ at the centre frequency $f_0 = \sqrt{f_{cR} \times f_{cL}}$ .

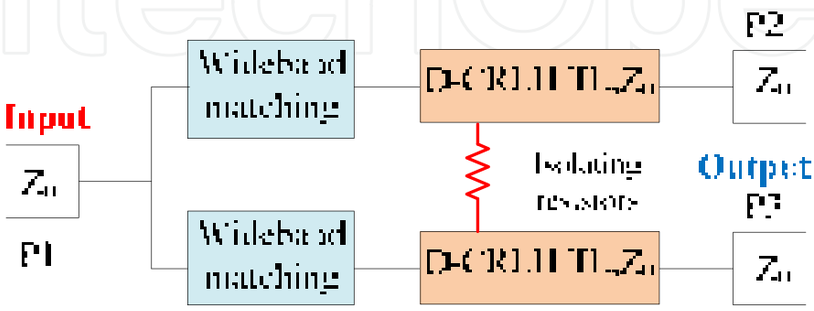


Fig. 25. D-CRLH TL power divider schematic diagram.

Fig. 26 shows the photograph of the fabricated D-CRLH transmission line power divider, in which there are five resistors with different values between the two D-CRLH transmission lines. They are simulated and optimized by IE3D to obtain the highest isolation between output ports. From left to right, the resistance values are 50 Ω, 100 Ω, 200 Ω, 400 Ω, and 800 Ω, respectively. The overall size of the power divider is about 50 mm × 40 mm.

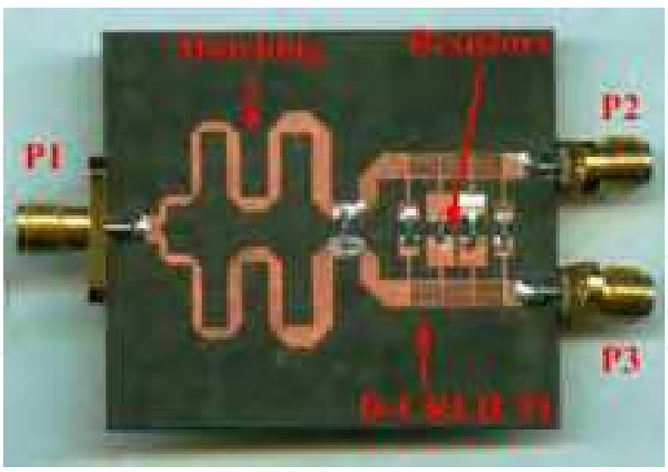


Fig. 26. Photograph of the fabricated D-CRLH transmission line power divider

The proposed power divider was measured using an Agilent N5230A vector network analyzer. The measured S-parameters of the design are illustrated in Fig. 27 (a). It can be seen the performance of the power divider is excellent. From 0.85 GHz to 4.3 GHz, $|S_{11}|$ is below -15 dB, the isolation is higher than 15 dB, and the insertion loss is less than 1 dB. Fig. 27 (b) shows the amplitude balance is below 0.3 dB between output ports, and the phase

balance is less than 3°. The bandwidth of the D-CRLH TL power divider is about five octaves. Thus, an ultra wide band is realized.
The simulated S-parameters of the design are illustrated in Fig. 28, which agree well with the measured results.

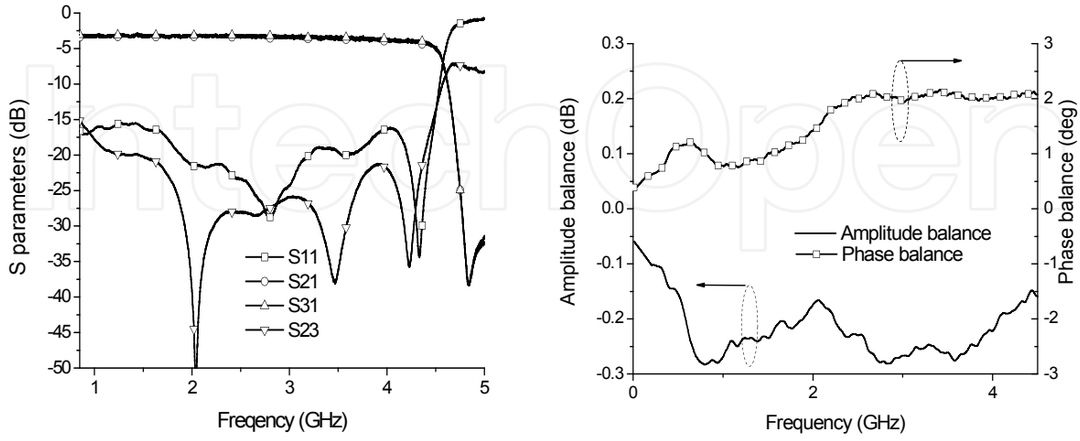


(a) S parameters (b) Amplitude balance and phase balance

Fig. 27. Measured results of the power divider

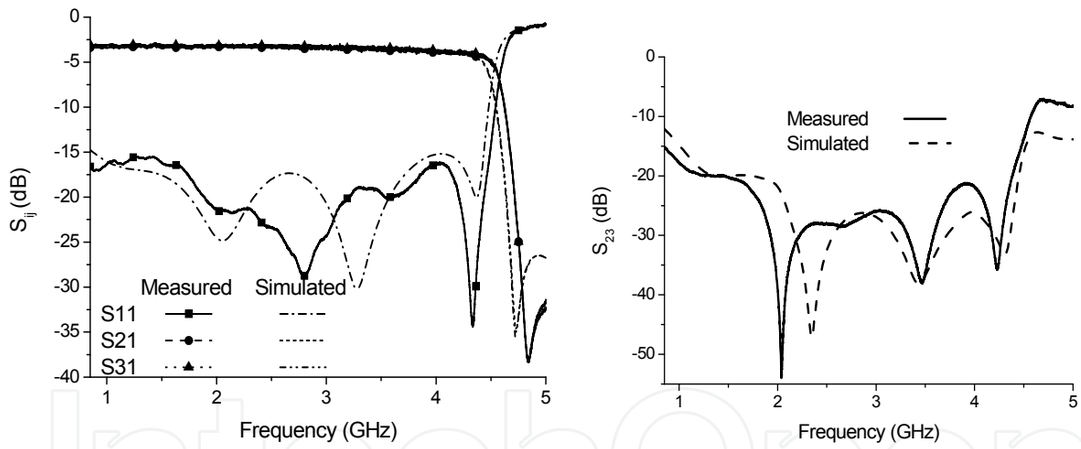


Fig. 28. Comparison between simulation and measurements

Compared with those of the conventional Wilkinson power dividers, the novel D-CRLH power divider obtains a bandwidth over 100% with reasonable return loss and isolation. Usually the bandwidth of a conventional Wilkinson power divider is about 20%. The insertion loss is less than power dividers based on CRLH transmission lines. The size of the proposed D-CRLH power divider is only about 70%. Thus, it is compact power divider with broadband width.
The novel 3 dB power divider based on dual-composite right/left handed transmission line has the feature of compact size, wide band, low insertion loss, high isolation, and good amplitude and phase balance. It can be applied to microwave signal separation, array antenna feed and so on.

Another scheme of power divider is to use the zeroth order resonance of a metamaterial transmission line. All output ports are in phase at the transition frequency. Due to the intrinsic parallel connection (the wavelength is infinite at the resonant frequency) in the power divider, the number of output ports is limited.
Multi-port power dividers based on metamaterial transmission lines are available as well. Based on the zeroth order resonance, the metamaterial transmission line shares the same phase at the transition frequency. Thus, an N-port power divider can be easily built, as shown in Fig. 29 (a) and (b). A metamaterial transmission line using ten series chip capacitors is used. The drawback of this power divider is the output impedance at each port is N times $Z_0$. A $\lambda_g/4$ impedance matching has to be applied. It limits the number of output ports. Meanwhile, the bandwidth of this power divider is much limited due to the zeroth order resonance.

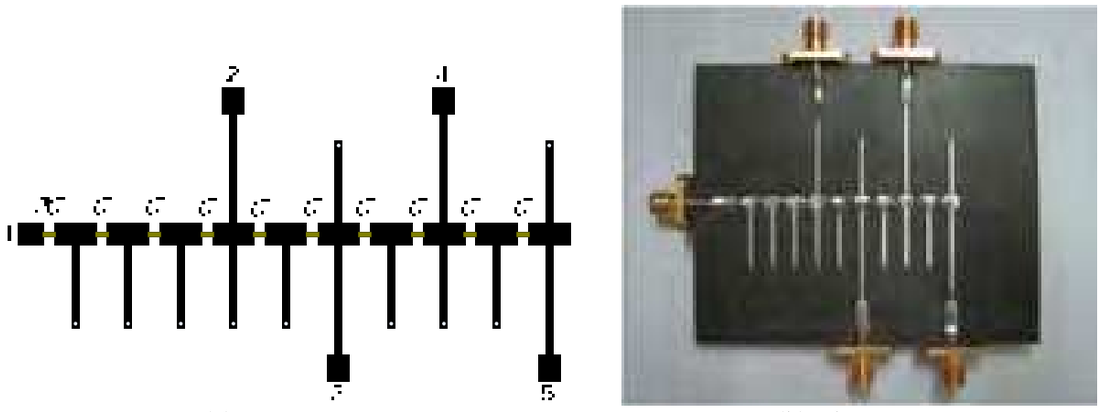

(a) Layout (b) Photo

Fig. 29. Layout and fabricated 1:4 power divider

A power divider based on a segment of metamaterial transmission line and three conventional microstrip lines, as shown in Fig. 31. Each unused conventional microstrip line end is connected with one match load. We assume that the coupling coefficients of those ideal couplers are C1, C2 and C3, respectively. The feeding power at port 1 is P1, and the output powers are P2, P3, P4, and P5 at the respective ports. When the reflection at port 1 and the insertion loss of the CRLH TL are neglected, the output powers are obtained as

$$\begin{cases} P_2 = P_1 - P_3 - P_4 - P_5 \\ P_3 = C_1 P_1 \\ P_4 = C_2 \left( P_1 - P_3 \right) \\ P_5 = C_3 \left( P_1 - P_3 - P_4 \right) \end{cases} \tag{8}$$

With careful design (choosing right coupler coefficients C1 to C3), the desired power division among port 2 to port 3 can be satisfied.

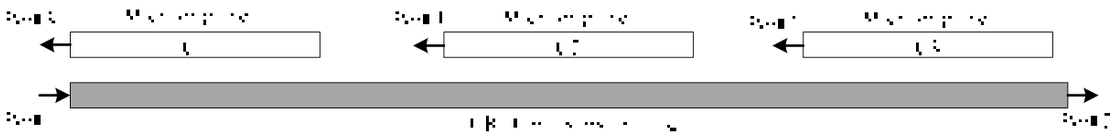

Fig. 30. Scheme of the proposed CRLH coupler. It is a 1:4 power divider, which contains one metamaterial transmission line and three conventional microstrip lines. Port 1 is input ports.

At the transition frequency of metamaterial transmission lines, there is no phase difference among their unit cells. Then, the outputs of a metamaterial coupler are in phase as well, since they have the same phase shift to the feeding port. Therefore, no phase adjusting is required in a metamaterial coupler based on the zeroth order resonance.

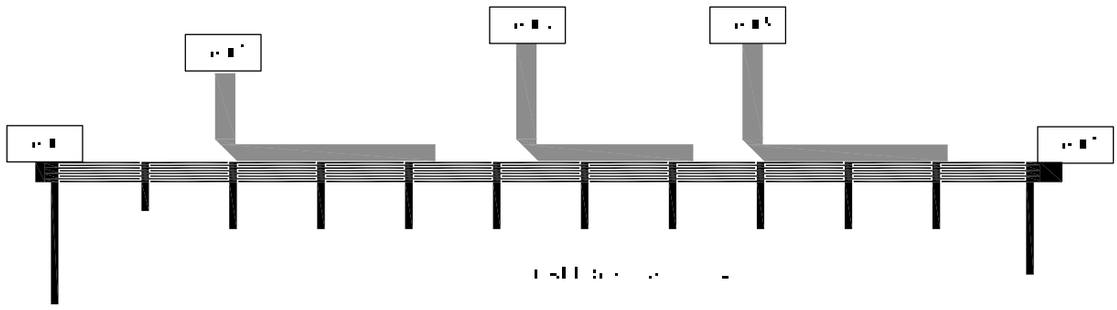

(a) Layout

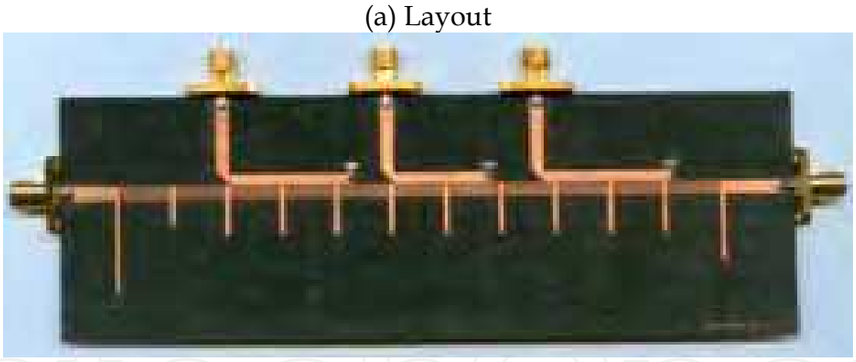

(b) Photo

Fig. 31. Layout of the proposed power divider based on CRLH couplers

The distance between the metamaterial transmission line and the coupling conventional microstrip transmission line is 0.15 mm. The layout of the proposed power divider based on metamaterial couplers is shown in Fig. 31 (a). The fabricated metamaterial power divider is shown in Fig. 31 (b). The substrate is F4B-2 with $\varepsilon_r = 2.65$ and thickness of 1 mm.

The unequal power division between port 2, port 3, port 4, and port 5 is designed to 4:2:1:1, in which the transmission from port 1 to those corresponding ports are -3 dB, -6 dB, -9 dB and -9 dB, respectively. The lengths of the coupling conventional microstrip transmission lines are adjusted to realize the desired unequal power division.

The simulated amplitude response is shown in Fig. 32 (a). At the transition frequency $f_0 = 2.4$ GHz, those transmitted amplitudes among output ports are -4.2 dB, -6.9 dB, -9.8 dB and -

9.8 dB. The reflection of port 1 at $f_0$ is -28 dB. The insertion loss is about 1.2 dB. For amplitude consideration, the reasonable bandwidth is about 500 MHz around the transition frequency. The problem is the coupled power at port 3 drops obviously when frequency is away from the transition frequency. A better bandwidth can be obtained with extra efforts to optimize the first coupler.

The phase shifts between output ports are shown in Fig. 31 (b). At transition frequency f0, all output ports share the same phase. Due to the dispersion characteristic of a CRLH TL, the bandwidth of ±10° is much narrower than the amplitude bandwidth. There is a phase difference of about 90° caused by the coupler. The microstrip TLs at port 3, port 4 and port 5 are extended to compensate the phase shift.

Transmissions between output ports are shown in Fig. 31 (c). The isolations between output ports are higher than 20 dB, as shown in Fig. 31 (c). Experimental results agree with the simulations well.

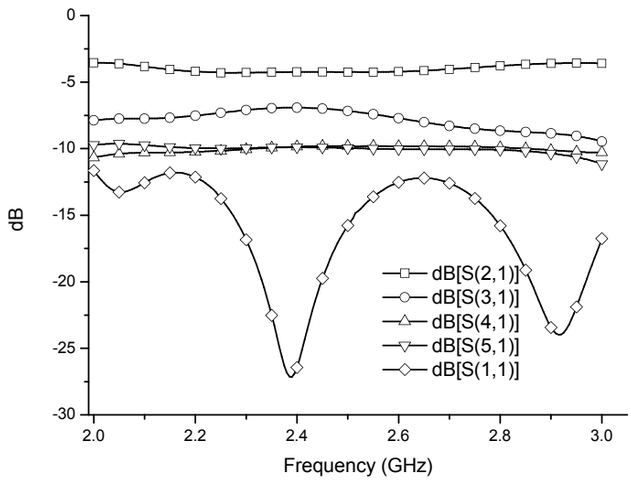


(a) Amplitude

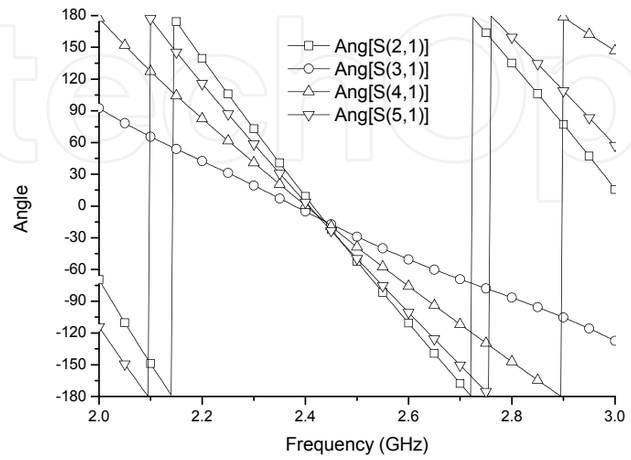


(b) Phase

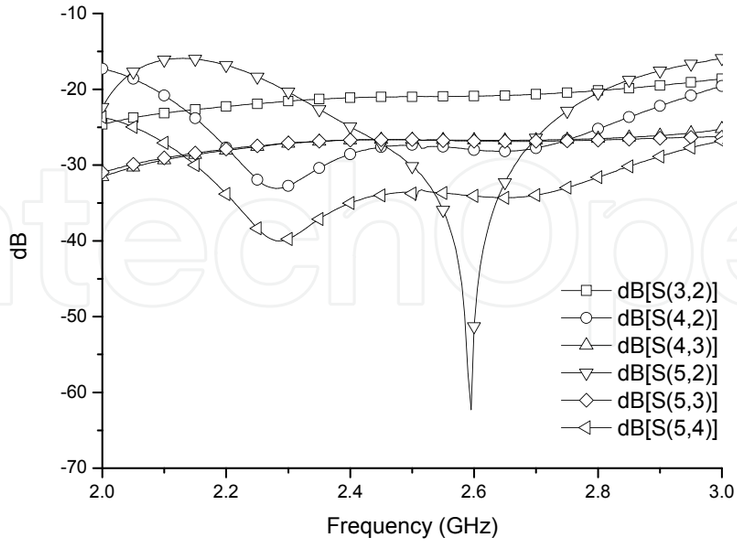


(c) Isolation

Fig. 32. Simulation results of the metamaterial power divider (© 2008 IEEE)

A novel unequal power divider based on the zeroth order resonance of a metamaterial transmission line is discussed. It is a miniaturized design along the longitudinal direction. The power divider can be easily extended to an arbitrary number of output ports. Not only even numbers but also odd numbers of output ports are suitable for the proposed power divider. Thus, the proposed power divider is a practical design.

Both equal and unequal power division are possible for the power divider. In further study, equal power divider will be considered and designed. Since the power divider is very compact along the longitudinal direction, it is suitable to realize an antenna feeding network. With desired unequal power division, an antenna array fed with the power divider may get arbitrary power supply.

The insertion loss of the metamaterial transmission at zeroth order resonance frequency is a little high. To reduce the insertion loss will make the new metamaterial power divider more reliable.

## 5. Conclusion

Metamaterial transmission lines are one-dimension structures. Their performances can be roughly analyzed by the circuit models, and the relation between them and band-pass filters is discussed as well. There are many applications of metamaterial transmission lines due to their excellent performance. Some typical applications, such as leaky-wave antenna, baluns, diplexers and power dividers are presented. Metamaterial transmission lines will find more and more applications of microwave components in future.

**Acknowledge**
This work was supported in part by the National Science Foundation of China under Grant 60971051 and the Youth Foundation of Sichuan Province under Grant 09ZQ026-016.

## 6. References

Caloz C. & Itoh T. (2006) *Electromagnetic metamaterials: Transmission line theory and microwave applications*. John Wiley & Sons, Inc. ISBN 0-471-66985-7; U.S.A.

Eleftheriades G.; Iyer A. & Kremer P. (2002). Planar negative refractive index media using periodically L-C loaded transmission lines, *IEEE Transaction on Microwave Theory and Technology*, Vol. 50, No. 12, 2702–2712, (Dec. 2002), ISSN 0018-9480

Eleftheriades G. & Balmain K. (2005) *Negative-Refraction metamaterials – Fundamental principles and applications*. John Wiley & Sons, Inc. ISBN 13: 978-0-471-60146-3; U.S.A.

Lai, A.; Itoh, T. & Caloz C. (2004). Composite right/left-handed transmission line metamaterial. *IEEE Microwave Magazine*, Vol. 5, No. 3, 34–50, (March 2004), ISSN 1527-3342

Liu, C. & Menzel, W. (2007). On the relation between a negative refractive index transmission line and Chebyshev filters, *Proceedings of the 37th European Microwave Conference*, pp. 704-707, ISBN 978-2-87487-001-9, October 2007, European Microwave Association, Munich, Germany

Liu, C. & Menzel, W. (2007). Frequency-scanned leaky-wave antenna from negative refractive index transmission lines, *Proceedings of the European Conference on Antennas and Propagation*, ISBN 978-0-86341-842-6, November 2007, European Association on Antennas and Propagation, Edinburg, UK

Liu, C. & Menzel, W. (2008). Broadband via-free microstrip balun using metamaterial transmission lines. *IEEE Microwave and Wireless Component Letters*, Vol. 18, No. 7, 437-439, (July 2008), ISSN 1531-1309

Wang, W.; Liu, C.; Yan, L. & Huang, K. (2009). A Novel Power Divider based on Dual-Composite Right/Left Handed Transmission Line. Journal of Electromagnetic Waves and Applications. Vol. 23, No. 8/9, 1173-1180, ( Sept. 2009), ISSN 0920-5071

Pozar, D. (2004). Microwave Engineering. John Wiley & Sons, Inc., ISBN 0-471-17096-8, U.S.A.

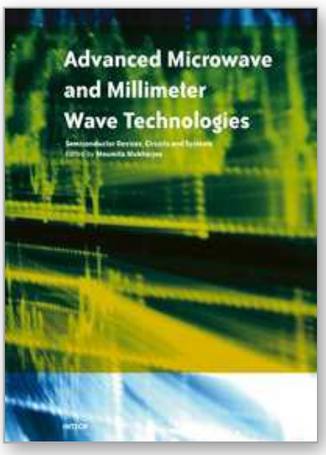


**Advanced Microwave and Millimeter Wave Technologies**
**Semiconductor Devices Circuits and Systems**
Edited by Moumita Mukherjee

ISBN 978-953-307-031-5
Hard cover, 642 pages
**Publisher** InTech
**Published online** 01, March, 2010
**Published in print edition** March, 2010

This book is planned to publish with an objective to provide a state-of-the-art reference book in the areas of advanced microwave, MM-Wave and THz devices, antennas and systemtechnologies for microwave communication engineers, Scientists and post-graduate students of electrical and electronics engineering, applied physicists. This reference book is a collection of 30 Chapters characterized in 3 parts: Advanced Microwave and MM-wave devices, integrated microwave and MM-wave circuits and Antennas and advanced microwave computer techniques, focusing on simulation, theories and applications. This book provides a comprehensive overview of the components and devices used in microwave and MM-Wave circuits, including microwave transmission lines, resonators, filters, ferrite devices, solid state devices, transistor oscillators and amplifiers, directional couplers, microstripeline components, microwave detectors, mixers, converters and harmonic generators, and microwave solid-state switches, phase shifters and attenuators. Several applications area also discusses here, like consumer, industrial, biomedical, and chemical applications of microwave technology. It also covers microwave instrumentation and measurement, thermodynamics, and applications in navigation and radio communication.



INTECH
open science | open minds

**InTech Europe**
University Campus STeP Ri
Slavka Krautzeka 83/A
51000 Rijeka, Croatia
Phone: +385 (51) 770 447
Fax: +385 (51) 686 166
www.intechopen.com

**InTech China**
Unit 405, Office Block, Hotel Equatorial Shanghai
No.65, Yan An Road (West), Shanghai, 200040, China
中国上海市延安西路65号上海国际贵都大饭店办公楼405单元
Phone: +86-21-62489820
Fax: +86-21-62489821

IntechOpen